Superconductivity in the PbO-type structure α-FeSe

Fong-Chi Hsu*†, Jiu-Yong Luo*, Kuo-Wei Yeh*, Ta-Kun Chen*, Tzu-Wen Huang*, Phillip M. Wu‡, Yong-Chi Lee*, Yi-Lin Huang*, Yan-Yi Chu*†, Der-Chung Yan*, and Maw-Kuen Wu*§

*Institute of Physics, Academia Sinica, Nankang, Taipei 115, Taiwan; †Department of Materials Science and Engineering, National Tsing Hua University, Hsinchu 30013, Taiwan; and ‡Department of Physics, Duke University, Durham, NC 27708

Contributed by Maw-Kuen Wu, July 28, 2008 (sent for review July 26, 2008)

The recent discovery of superconductivity with relatively high transition temperature (Tc) in the layered iron-based quaternary oxypnictides La[$O_{1-x}F_x$] FeAs by Kamihara *et al.* [Kamihara Y, Watanabe T, Hirano M, Hosono H (2008) Iron-based layered superconductor La[O1-xFx] FeAs (x = 0.05–0.12) with Tc = 26 K. *J Am Chem Soc* 130:3296–3297.] was a real surprise and has generated tremendous interest. Although superconductivity exists in alloy that contains the element Fe, LaOMPn (with M = Fe, Ni; and Pn = P and As) is the first system where Fe plays the key role to the occurrence of superconductivity. LaOMPn has a layered crystal structure with an Fe-based plane. It is quite natural to search whether there exists other Fe based planar compounds that exhibit superconductivity. Here, we report the observation of superconductivity with zero-resistance transition temperature at 8 K in the PbO-type α-FeSe compound. A key observation is that the clean superconducting phase exists only in those samples prepared with intentional Se deficiency. FeSe, compared with LaOFeAs, is less toxic and much easier to handle. What is truly striking is that this compound has the same, perhaps simpler, planar crystal sublattice as the layered oxypnictides. Therefore, this result provides an opportunity to better understand the underlying mechanism of superconductivity in this class of unconventional superconductors.

electronic properties | Fe-oxypnictide

Although superconductivity exists in alloy (1) that contains the element Fe, LaOMPn (2–9) (with M = Fe, Ni; and Pn = P and As) is the first system where Fe plays the key role in the occurrence of superconductivity. LaOMPn has a layered crystal structure with an Fe-based plane. It is quite natural to ask whether other Fe-based planar compounds exist that exhibit superconductivity. Here, we report the observation of superconductivity with zero resistance transition temperature at 8 K in the PbO-type α-FeSe compound. Although FeSe has been studied quite extensively (10, 11), a key observation is that the clean superconducting phase exists only in those samples prepared with intentional Se deficiency.

FeSe comes in several phases: (*i*) a tetragonal phase α-FeSe with PbO-structure, (*ii*) a NiAs-type β-phase with a wide range of homogeneity showing a transformation from hexagonal to monoclinic symmetry, and (*iii*) an $FeSe_2$ phase that has the orthorhombic marcasite structure. The most studied of these compounds are the hexagonal Fe_7Se_8, which is a ferrimagnet with Curie temperature at ≈125 K, and monoclinic Fe_3Se_4.

Unlike the high-temperature (high-Tc) superconductors (12) discovered >20 years ago that have a CuO_2 plane that is essential for the observed superconductivity, the tetragonal phase α-FeSe with PbO structure has an Fe-based planar sublattice equivalent to the layered iron-based quaternary oxypnictides, which have a layered crystal structure belonging to the P4/nmm space group (2). The crystal of α-FeSe is composed of a stack of edge-sharing $FeSe_4$-tetrahedra layer by layer, as shown schematically in Fig. 1. Polycrystalline samples with nominal concentration $FeSe_{1-x}$ (x = 0.03 and 0.18) were synthesized and studied. X-ray diffraction analysis of the samples in Fig. 2 shows that α-FeSe is dominant, and β-FeSe phases exist in trace amounts. This result is reasonable because in the Fe-Se binary alloy system, the

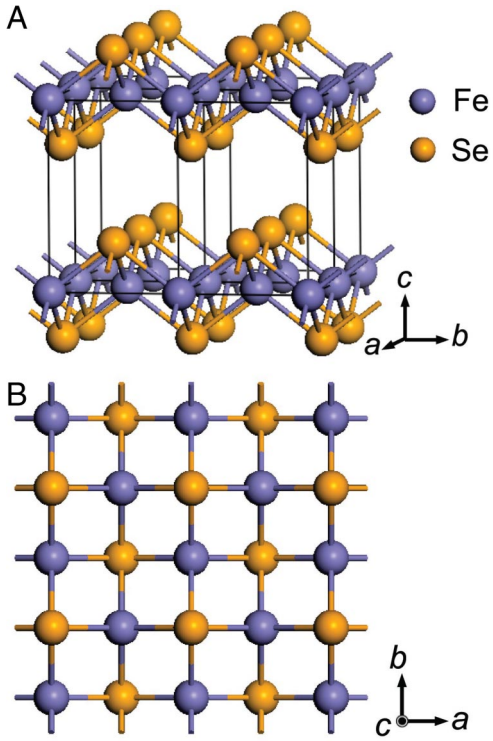

Fig. 1. Schematic crystal structure of α-FeSe. Four unit cells are shown to reveal the layered structure.

α-phase is considered as a slightly Se-deficient phase [45–49.4 atomic percent (at%) Se] and the β-phase, in contrast, persists in a wide range of compositions from slightly Fe-rich to Se-rich (49.5–58 at% Se) (13). In $FeSe_{0.82}$, the possible iron oxide impurity phases could come from either starting materials (99.9% Fe) or surface oxidation during sintering, and the silicides might be the product of reactions between the sample and silica ampoules. Nevertheless, the samples contained only trace amounts of these impurity phases (note that the y axis of Fig. 2 is in log scale). The calculated lattice constants are a = 0.37693 (1) nm and c = 0.54861 (2) nm for $FeSe_{0.82}$, and a = 0.37676 (2) nm and c = 0. 54847 (1) nm for $FeSe_{0.88}$. The lattice constant slightly expands in the a axis and shrinks in the c axis for both samples as compared with those of α-FeSe in the Joint Committee on Powder Diffraction Standards Card (85-0735, unpublished) (13) (a = 0.3765 nm and c = 0.5518 nm). This

Author contributions: M.-K.W. designed research; F.-C.H., J.-Y.L., K.-W.Y., T.-K.C., T.-W.H., P.M.W., Y.-C.L., Y.-L.H., Y.-Y.C., and D.-C.Y. performed research; F.-C.H., J.-Y.L., K.-W.Y., T.-K.C., T.-W.H., P.M.W., Y.-C.L., Y.-L.H., Y.-Y.C., D.-C.Y., and M.-K.W. analyzed data; and P.M.W. and M.-K.W. wrote the paper.

The authors declare no conflict of interest.

Freely available online through the PNAS open access option.

§To whom correspondence should be addressed. E-mail: mkwu@phys.sinica.edu.tw.

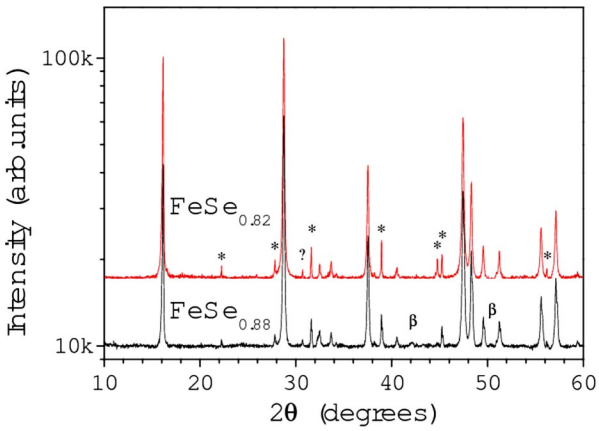

Fig. 2. Powder x-ray diffraction patterns of $FeSe_{0.82}$ and $FeSe_{0.88}$. The patterns show that the resulting sample with starting composition of Fe (53%)/Se (47%) composes of primarily PbO-type tetragonal $FeSe_{1-x}$ (P4/nmm), the α-phase, and partly of NiAs-type hexagonal FeSe (P63/mmc), the β-phase. The sample with higher initial iron content, Fe (55%)/Se (45%), shows no β-phase but trace amounts of possible impurity phases including elemental selenium, iron oxide, and iron silicide (marked with an asterisk). Question marks in the figure represent unknown phases.

lattice distortion is most probably due to the deficiency of Se, and this gives a quick estimate of the difference in selenium concentration between $FeSe_{0.82}$ and $FeSe_{0.88}$.

Fig. 3 displays the temperature dependence of electrical resistivity (ρ) of $FeSe_{0.88}$. The resistivity shows a broad bump at ≈250 K and exhibits metallic characteristics before the onset of the superconducting transition. The room temperature-to-residual resistance ratio is ≈6. Interestingly, an anomalous downturn in resistivity at ≈100 K is observed. As the temperature is lowered further, the zero-resistance transition occurs at ≈8 K. The transition width is rather broad, suggesting the inhomogeneous nature of the sample. Superconducting critical transition temperature (Tc) in variety of applied magnetic field up to 9 T was determined by taking the temperature where the resistance drops to 50% of that at the onset (50% Rn). Fig. 3 *Left Inset* shows the resistive measurements at various magnetic field strengths. The *Right Inset* of Fig. 3 shows the temperature dependence of the upper critical field, and the experimental

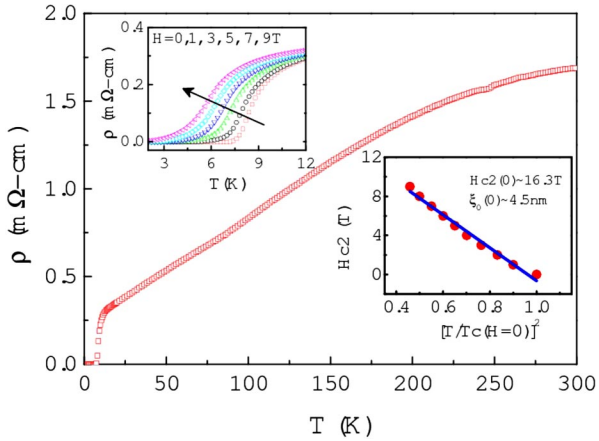

Fig. 3. Temperature dependence of electrical resistivity (ρ) of $FeSe_{0.88}$. The *Left Inset* shows the resistive measurement in magnetic fields (H) of 0, 1, 3, 5, 7, and 9T below 12 K. Tc decreases linearly with increasing magnetic field. The *Right Inset* displays the temperature dependence of upper critical field (Hc2), with the fit shown in blue.

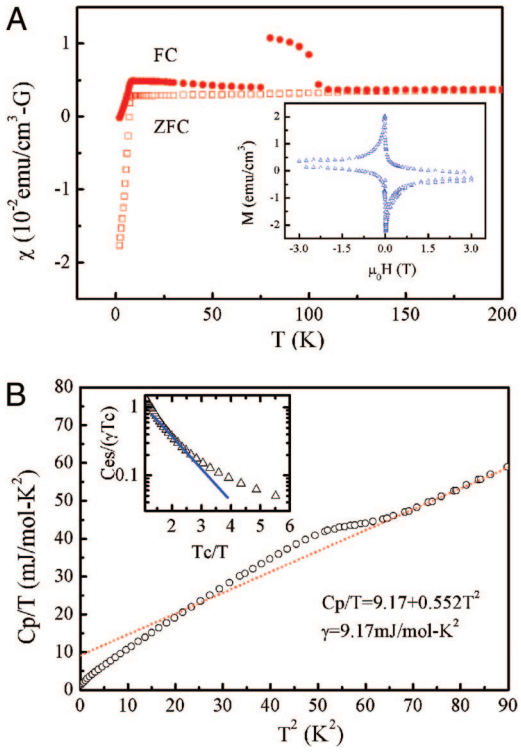

Fig. 4. Magnetic susceptibility and specific heat of $FeSe_{0.88}$. (*A*) Temperature dependence of magnetic susceptibility measured in a 30-G magnetic field. A small magnetic anomaly is observed at ≈105 K, which is more pronounced in the FC measurements. *Inset* shows the magnetic hysteresis of the sample measured at 2 K. It confirms the superconducting characteristic of the sample. (*B*) Low temperature-specific heat of $FeSe_{0.88}$. The red dotted line is the curve fitting of phonon and electronic contribution to the specific heat. The intercept at zero temperature gives γ = 9.17 mJ/mole-K^2. A specific jump appears at ≈8 K, which coincides with the zero-resistance temperature that confirms the superconducting transition. The *Inset* shows the semilogarithmic Ces/γTc vs. Tc/T in the superconducting state. The measured plot displays deviation from the linear curve of the fully gapped superconductor (solid blue straight line).

result was fit to the relationship, Hc2/Hc2 (0) = 1 − (T/Tc (0))^2, shown by the blue line. The estimated upper critical field Hc2 (0) is ≈16.3 T, which gives a coherence length ξ_0 ≈ 4.5 nm.

The magnetic susceptibility as a function of temperature was measured at 30-G field strength, as shown in Fig. 4*A*. The zero field cool (ZFC) susceptibility is essentially temperature independent, indicating that the sample is a Pauli paramagnet before the onset of superconductivity. A sharp drop, indicating the magnetic onset of superconductivity, appears at ≈8 K, which is the same as the zero-resistance temperature. The susceptibility shows a relatively large Pauli susceptibility in the normal state. This relatively large positive background above Tc can possibly be attributed to the existence of trace Fe impurity. A relatively small magnetic anomaly occurs at ≈105 K, which is more pronounced in the field-cool measurement. This magnetic anomaly occurs at the same temperature as that observed in the resistive measurement. Further confirmation of superconductivity is shown in the *Inset* of Fig. 4*A*, which displays the typical magnetic hysteresis curve for a superconductor. Fig. 4*B* shows the specific heat of the $FeSe_{0.88}$ sample. In the normal state, the electronic coefficient of specific heat γ = 9.17 mJ/mol-K^2, which can be seen from the zero-temperature intercept. The superconducting transition at Tc is relatively broad, and the estimated ΔCp/γTc is ≈0.61. In the superconducting state, the best fit of data over the temperature range $1 < Tc/T < 1.8$ leads to Ces/γTc = 7.69exp(−1.58Tc/T). But it does not follow the BCS relation over the full temperature range below Tc, as shown in the

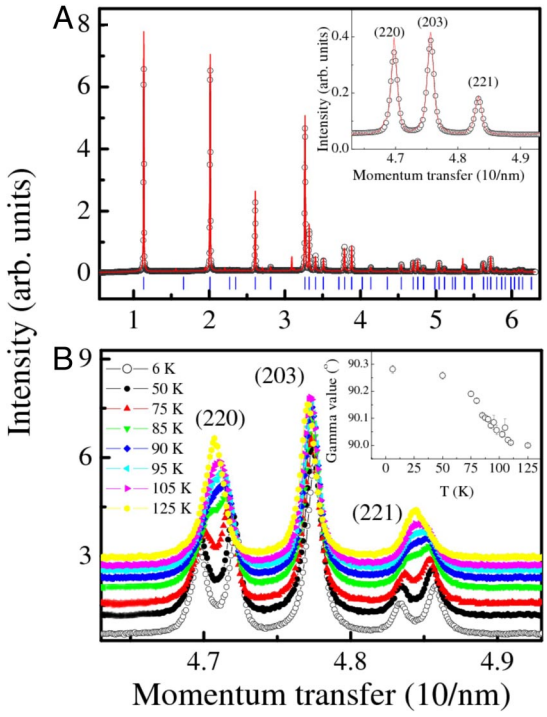

Fig. 5. The moment transfer is $M = 4\pi\sin(\theta)/\lambda$. (*A*) Observed (open black circle) and calculated (red solid line) powder diffraction intensities of $FeSe_{0.88}$ at 300 K using space group P4/nmm. The *Inset* in *A* shows a single peak of the (2, 2, 0), (2, 0, 3), (2, 2, 1) reflection at room temperature. But double peaks show up for (2, 2, 0) and (2, 2, 1) at low temperature, as seen in *B*. The double-peak structure begins to show up at ≈105 K. *Inset* in *B* shows the temperature dependence of the γ angle fit with P-1 symmetry.

Inset of Fig. 4*B*. This result may originate from the presence of impurity phases in the final product. However, it may also imply that the $FeSe_{1-x}$ is possibly an unconventional superconductor.

Recently, it was reported (14, 15) that a pseudogap exists in La(O-F)FeAs, similar to that of the high-Tc cuprates, based on the temperature-dependent laser photoemission spectroscopy (PES). On the other hand, Mössbauer experiments (16) suggested that the suppression of magnetic and structural transition by F-doping in the LaOFeAs system may play the key role in the observation of superconductivity. It is possible that the anomaly observed in both the magnetic and resistive measurements in the $FeSe_{1-x}$ system may have similar origin. In fact, high-resolution x-ray diffraction experiments at low temperature indeed show the presence of a structural transformation at ≈105 K. Fig. 5 shows the diffraction patterns of the sample at different temperatures. At 300 K, a single peak of the (2, 2, 0), (2, 0, 3), (2, 2, 1) reflection is seen (Fig. 5*A Inset*), but clear splitting of the diffraction peaks into two peaks is observed below ≈105 K, Fig. 5*B*. Detailed refinement of the diffraction data suggests that the crystal structure changes from the tetragonal (P4/nmm) symmetry to the triclinic (P-1) symmetry, with the lattice parameters at 6 K of $a = 0.3773$ nm, $b = 0.3777$ nm, $c = 0.5503$ nm; both angles α and β remain at 90°, but the γ-angle increases from 90 to ≈90.3°. Fig. 5*B Inset* shows the temperature dependence of γ-angle fit with P-1 symmetry. Whether this observed structural change at low temperature is related to the appearance of superconductivity is currently under intensive investigation. In summary, we have confirmed the existence of superconductivity in the binary alloy $FeSe_{1-x}$ that exhibits PbO-type structure. Transport measurements show that the upper critical field of these compounds is in the order of 17 T, which implies a coherence length of ≈40 Å. In the superconducting state, the specific heat data can only fit to the BCS relation over a relatively narrow range, $1 < Tc/T < 1.8$. This observation suggests that superconductivity in $FeSe_{1-x}$ is most likely unconventional. An interesting low-temperature phase transition at ≈100 K from P4/nmm symmetry to P-1 symmetry was observed. This structural change, which only affects the lattice parameters without breaking the magnetic symmetry, may strongly correlate with the origin for superconductivity.

Materials and Methods

Polycrystalline bulk samples were prepared with the following procedure. High-purity (99%) powder of selenium and iron with appropriate stoichiometry ($FeSe_{1-x}$ with $x \approx 0.03$–0.18) were mixed and ground with an agate mortar and pestle. The grinding process was carried out in a fume hood with strong ventilation. The ground powder was cold-pressed into discs with 400 kg/cm^2 uniaxial stress. The discs were sealed in an evacuated quartz tube (in 10 −5-torr vacuums) and slowly ramped to 700°C, which is a little above the boiling point of Se, at the rate of 100°C/hr. Finally, the temperature was kept at 700°C for 24 h. After cooling to room temperature at the rate of 300°C/hr, the loose sample was reground, pressed, sealed in a quartz tube, sintered again at 700°C for 24 h, and finally annealed at 400°C for 36 h. All of the samples were kept in vacuum dessicators before measurement. The sample resistance was measured by using the standard four-probe method using silver paste for contact. Measurements were carried out with a Quantum Design Physical Property Measurement System (model 6000; PPMS) (Fig. 3). DC magnetic susceptibility measurements were performed in a Quantum Design superconducting quantum interference device vibrating sample magnetometer (SQUID-VSM) (Fig. 4*A*). The $FeSe_{0.88}$ powder sample was measured in two ways: (*i*) the sample was cooled without an initial external magnetic field applied (ZFC, open squares) and (*ii*) then cooled in an initial external magnetic field (FC, solid squares). After initializing, a 30-G magnetic field was applied, and the susceptibility was measured as a function of temperature. Low temperature-specific heat measurements were carried out with thermal relaxation method in a zero magnetic field (Fig. 4*B*). For powder diffraction measurements, a Philips PW3040/60 diffractometer with x-ray (Cu, $K\alpha = 1.5418$ Å) radiation was used for phase identification of the sample (Fig. 2). The temperature dependence of the x-ray powder diffraction (Fig. 5) was measured by using the synchrotron source at BL12b2 in SPring 8 with incident beam wavelength of 0.995 Å.

ACKNOWLEDGMENTS. We acknowledge fruitful discussions with T. K. Lee and Sungkit Yip. This work was partially supported by a National Science Council of Taiwan Grant and the U.S. Air Force Office of Scientific Research through its Tokyo Asian Office of Aerospace Research and Development Grant 084049.

1. Unruh KM, Chien CL (1984) Magnetic properties and hyperfine interactions in amorphous Fe-Zr alloys. *Phys Rev B* 30:4968–4974.
2. Kamihara Y, Watanabe T, Hirano M, Hosono H (2008) Iron-based layered superconductor La[O1-xFx] FeAs (x = 0.05–0.12) with Tc = 26 K. *J Am Chem Soc* 130:3296–3297.
3. Takahashi H (2008) Superconductivity at 43 K in an iron-based layered compound LaO1-xFxFeAs. *Nature* 453:376–378.
4. Chen GF, *et al.* (2008) Superconductivity at 41 K and its competition with spin-density-wave instability in layered CeO1-xFxFeAs. *Phys Rev Lett* 100:247002.
5. Chen XH, *et al.* (2008) Superconductivity at 43 K in samarium-arsenide oxides SmFeAsO1-xFx. *arXiv*: 0803.3603v2.
6. Cheng P, *et al.* (2008) Superconductivity at 36 K in gadolinium-arsenide oxides GdO1-xFxFeAs. *Sci Chin G* 51:719–722.
7. Wen HH, *et al.* (2008) Superconductivity at 25K in hole-doped (La1-xSrx)OfeAs. *Europhys Lett* 82:17009.
8. Yang J, *et al.* (2008) Superconductivity at 53.5 K in GdFeAsO1-x. *Supercond Sci Technol* 21:082001.
9. Ren ZA, *et al.* (2008) Superconductivity at 55 K in iron-based F-doped layered quaternary compound Sm[O1-xFx]FeAs. *Chin Phys Lett* 25:2215.
10. Terzieff P, Komarek KL (1978) The paramagnetic properties of iron selenides with NiAs-type structure. *Monats Chem* 109:651–659.
11. Schuster W, MiMer H, Komarek KL (1979) Transition metal–chalcogen systems, VII: the iron–selenium phase diagram. *Monats Chem* 110:1153–1170.
12. Wu MK, *et al.* (1987) Superconductivity at 93K in a new mixed phase Y-Ba-Cu-O compound system at ambient pressure. *Phys Rev Lett* 58:908–910.
13. Okamoto H (1991) The Fe–Se (iron–selenium) system. *J Phase Equilibria* 12:383–389.
14. Ishida Y, *et al.* (2008) Evidence for pseudogap evolutions in high-Tc iron oxypnictides. *arXiv*:0805.2647v1.
15. Sato T, *et al.* (2008) Superconducting gap and pseudogap in iron-based layered superconductor La(O1-xFx)FeAs. *J Phys Soc Jpn* 77:063708.
16. Kitao S, *et al.* (2008) Spin ordering in LaOFeAs and its suppression in superconductor LaO0.89F0.11FeAs probed by Mösssbauer spectroscopy. *J Phys Soc Jpn*.